The November 2017 Mw 5.5 Pohang earthquake: A possible case of induced seismicity in South Korea

F. Grigoli[1]*, S. Cesca[2], A. P. Rinaldi[1], A. Manconi[3], J. A. López-Comino[2], J. F. Clinton[1], R. Westaway[4], C. Cauzzi[1], T. Dahm[2] and S. Wiemer[1]

Affiliations:

[1] ETH-Zurich, Swiss Seismological Service, Zurich, Switzerland
[2] GFZ-Potsdam, Section 2.1: Earthquake and Volcano Physics, Potsdam, Germany
[3] ETH-Zurich, Department of Earth Sciences, Engineering Geology, Zurich, Switzerland
[4] University of Glasgow, School of Engineering, Glasgow, UK

*Correspondence to: francesco.grigoli@sed.ethz.ch

Abstract: The M_w 5.5 earthquake that struck South Korea in November 2017 was one of the largest and most damaging events in this country over the last century. Its proximity to an Enhanced Geothermal Systems site, where high pressure hydraulic injection had been performed during the previous two years, raises the possibility that this earthquake was anthropogenic. We have combined seismological and geodetic analyses to characterize the mainshock and its largest aftershocks, constrain the geometry of this seismic sequence and shed light on its casual factors. According to our analysis it seems plausible that the occurrence of this earthquake was influenced by these industrial activities. Finally we found that the earthquake transferred static stress to larger nearby faults, potentially increasing the seismic hazard in the area.

One sentence summary: A detailed analysis of the November 15, 2017, Mw 5.5 South Korea earthquake shows a potential link with proximal hydraulic stimulation operations for geothermal energy exploitation.

Main Text: Deep geothermal resources can give a valuable contribution to the production of renewable energy. Through Enhanced Geothermal Systems (EGS), geothermal energy production is no longer confined to volcanic or hydrothermal regions. EGS technologies, unlike the conventional geothermal systems, exploit geothermal resources through hydraulic stimulation, which involves injecting pumping high-pressure cold water

to increase the permeability of the target formation at a few kilometers depth, by creating new fractures or enhancing existing ones. While the potential for deep geothermal energy is indisputably large, in urban areas the problem of induced seismicity associated with such operations is often not adequately addressed.

On November 15, 2017, a Mw 5.5 earthquake struck South Korea, injuring about 70 people and causing extensive damage in and around the city of Pohang. This earthquake was preceded by the Mw 5.5 Gyeongju event of September 12, 2016, which occurred ~30 km farther south on a major right-lateral fault, the Yangsan Fault, which continues northward through the Pohang area (1,2) (Fig. 1A and 1B). These earthquakes are the largest recorded in South Korea since instrumental monitoring of seismicity began in 1903 (2). The proximity to an EGS site (Fig. 1B), where hydraulic stimulation operations had recently taken place, has led to a public debate in South Korea regarding the potential anthropogenic origin of the 2017 Pohang earthquake. Between early 2016 and September 2017, many thousands of cubic meters of water were injected under pressure at this site into wells reaching ~4 km depth (3). An investigation by the South Korean government is currently ongoing, but we present observations that suggest a causal connection between the EGS activity and the most recent large earthquake.

The Korean Peninsula is generally considered stable with low to moderate intraplate seismic activity, but historical seismicity of this region indicates large secular variations in earthquake rate and energy release (4,5). The relatively low activity since 1904 was preceded by much higher activity between the 15th to 18th centuries, with a peak of 1000 reported historical earthquakes between 1500 and 1600 AD (5). The largest events reached magnitude ~7 (4,5). The historic earthquakes were likely associated with the major fault systems of the area, such as the Yangsan Fault, and highlight that these structures are active (4,5). In principle, given the historically varying rates of seismicity and prevalence of faults in this region, the increase represented by the 2016 Gyeongju and 2017 Pohang earthquakes is not completely inconsistent with the historically varying rates of seismicity. This leaves open the possibility that the occurrence of earthquakes close to the EGS site is a coincidence.

We applied full-waveform seismological methods to regional and teleseismic data (Fig. 1A, 6) as we do not have access to open data from a local seismic network (with the exception of two accelerometers deployed in the epicentral area). We analyzed 15 days of continuous waveform data covering November 15-30. We detected and relocated 46 events, most with magnitude M > 2. The trend of these 46 epicenters indicates a WSW-ENE strike of the fault that ruptured in the mainshock (Fig. 2A). We determined 3-7 km hypocentral depths for most of these events (Fig. 2A). This depth is shallower than typical seismicity in the area which is of about ~12-15 km (Fig 2B, 2,4). We determined the depth of both the mainshock and largest aftershock of the Pohang earthquake as 4.0-4.5 km (Fig. 2A). Depth is a critical parameter for discrimination between natural and induced seismicity (7), so we obtained independent estimates (we used array analysis at telesesismic distances and two accelerometers located in the epicentral region) that confirm the shallow depth (6). Our moment tensor inversion indicated that the mainshock had a reverse-faulting to oblique double couple (DC) mechanism, with a WSW-ENE striking nodal plane, subparallel to the aftershock zone, and dipping NNW at ~66°. The full moment tensor had a large non-DC term. Conversely, the Mw 4.3 aftershock indicated reverse-faulting on a WSW-ENE striking fault (Figs. 1B and 2A). Based on many previous analyses (e.g. (8,9)), we inferred that the non-DC component (Fig. 2A) is caused by a complex rupture process that includes the (near-)simultaneous activation of differently oriented faults. By mapping the azimuthal distribution of the apparent source durations, maximum energy peaks and centroid time delays, we retrieve a common pattern, which we interpret as the failure of two subevents at close origin times and separated by small distance along the azimuth of rupture directivity. We estimated a distance of 3.5-4.0 km between the two subevents, suggesting a dynamic triggering process (6). We thus hypothesize that the earthquake involved the failure of two different faults with slightly different orientations, which might in principle explain the non-DC term of the moment tensor (9), as well as the complexity of P wave signals for the mainshock (6). A potential, alternative source model, characterized by a complex rupture along a single fault, with heterogeneous slip directions, cannot explain the non-DC component of the moment

tensor and gives a significantly worse fit for the pattern of the relative hypocentral-centroid location (6).

We also used satellite radar interferometry (Differential InSAR - DInSAR) to map and measure the coseismic surface deformation associated with the mainshock and to independently model its source geometry (10,6). Our InSAR analysis indicated maximum surface deformation of ~5 cm, with a fault location and area consistent with the seismological analysis (Fig. 3A). Despite the moderate event size and complex rupture resolved by seismological data, we can fit the observed deformation with a simple elastic dislocation model (11) based on a single fault plane with shear displacement and opening (Fig. 3B). The fault dimensions (length ~5 km and width ~1.6 km) and the apparent slip, derived from this inversion of geodetic data are compatible with a magnitude of Mw 5.5 (12) and consistent with our seismological analysis. However, DInSAR data cannot resolve the small-scale complexities associated with the progressive rupture of adjacent fault patches. Nonetheless, our geodetic analysis confirmed that the earthquake nucleation and main slip on the fault occurred at very shallow depth (4-5 km), on a reverse fault striking WSW-ENE and with a ~75° dip towards the NW (Fig. 2C). The average residuals are ~0.05 cm and within the measurement accuracy (Fig. 3B). The DInSAR results are in good agreement with the aftershock locations and the focal mechanisms of the largest events, placing strong independent constraints on the location and extent of a previously unknown fault system.

Natural and induced earthquakes are indistinguishable using their waveform characteristics. Distinguishing induced earthquakes typically relies on building a convincing chain of evidence (7,13,14,15,16). The hypothesis that the Pohang earthquake sequence is anthropogenic is supported by the spatial correlation between the mainshock and its aftershocks and the injections. Our seismological and geodetic analyses indicate that the activated fault passes directly beneath the EGS site (Fig. 2C), within ~1 km of the termination of the injection wells (Fig. 2c). The combined evidence from the hypocentral locations, the DInSAR data inversion, the observed interval between P- and S- wave arrival times at the borehole and surface station, and the observed strong

motion and damage patterns are all consistent with this interpretation (6). Another piece of evidence supporting that this seismicity is induced is our re-location of the ML 3.1 earthquake on April 15, 2017, which occurred during hydraulic stimulation operations at the EGS site: this event was very close to the November 15 mainshock (Fig. 2A). No stimulation activities occurred in the two months preceding this mainshock, but induced earthquakes can be delayed by days, weeks, or even months after the start/end of injection (14). Our techniques (using regional and teleseismic data from the public domain, thus restricted to earthquakes of magnitude ≥~2) demonstrates the extent to which a candidate case study of induced seismicity can be investigated using public data, without proprietary data from site operators.

Another issue concerns the relation between the seismic moment (M_o ~1.7×10^{17} Nm) of the mainshock (6) and the volume V of fluid injected. We estimated an upper bound to the total volume of ~10,000 m3 based on the assumption that unreported injections are similar to initial stimulation (3). The limitation of water supply and storage capacity of the EGS justifies our assumption. We approximated an upper bound to M_o using the product of net injected volume and the shear modulus (17). For V=10,000 m^3 this relation implies an upper bound of M_o of ~2×10^{14} Nm, or M_w ~3.5. On this basis an induced earthquake of M_w 5.5 would require three orders of magnitude more volume (V ~10^7 m^3). Several counterexamples exist to this scaling relation (18, 19 and references therein) and the Pohang earthquake provides a much clearer evidence, suggesting that its use should be subject to caution.

While none of our observations exclude the possibility that the Pohang earthquake was induced by the EGS, our seismological and geodetic analysis (Figs 2-3) rules out a re-activation of the Yangsan fault. Our hypocenter is <1 km SE of the injection point, at the same depth as the injection. Co-seismic deformation and source model derived from the DInSAR analysis confirm this location (Figs 2-3). Aftershock locations, and focal mechanisms consistently indicate activation of a previously unknown fault system. This case thus highlights the importance of a preliminary seismo-tectonic assessment of the area surrounding any future EGS project site, aimed at identifying potentially active faults

Along with real-time analysis and control systems (20), this may mitigate the risk associated with induced seismicity.

We also investigate whether the September 2016 Mw 5.5 Gyeonju earthquake might have contributed to triggering the 2017 Pohang event. Coulomb stress modelling (6) indicates that the Gyeonju earthquake caused a slight (~0.0005 MPa) increase in static stress on the fault that ruptured in the subsequent Pohang earthquake. This value is small but it is feasible to propose a clock-advance on the subsequent fault occurred. In turn, the Mw 5.5 Pohang earthquake transferred static stress of 0.015 MPa onto the northern part of the Yangsan Fault (Fig. 4B) potentially increasing the seismic hazard in this area.

In conclusion, it is plausible that the occurrence of the Pohang earthquake was influenced by the nearby stimulation activities. If so, it was the largest and most damaging earthquake ever to have been associated with EGS, making it a potential 'game changer' for the geothermal industry worldwide.

References:

1. Y. Kim, X. He, S. Ni, H. Lim, S. C. Park, Earthquake source mechanism and rupture directivity of the 12 September 2016 Mw 5.5 Gyeongju, South Korea, earthquake. *Bulletin of the Seismological Society of America*, **107**(5), 2525-2531 (2017).

2. K. H. Kim, J. Kim, M. Han, S. Y. Kang, M. Son, T. S. Kang, J. Rhie, Y. H. Kim, Y. Park, H. J. Kim, Q. You, T. Hao. Deep Fault Plane Revealed by High‐ Precision Locations of Early Aftershocks Following the 12 September 2016 ML 5.8 Gyeongju, Korea, Earthquake. *Bulletin of the Seismological Society of America, **108(1),** 517-523 (2017).*

3. S. Park, L. Xie, K. Kim, S. Kwon, K. Min, J. Choi, W. S. Yoon, Y. Song, First Hydraulic Stimulation in Fractured Geothermal Reservoir in Pohang PX-2 Well, *Procedia Engineering, **191**, 829-837 (2017).*

4. M. Han, K. H. Kim, M. Son, S. Y. Kang. Current microseismicity and generating faults in the Gyeongju area, southeastern Korea. *Tectonophysics*, **694**, 414-423 (2017).

5. K. Lee, W. S. Yang. Historical seismicity of Korea. *Bulletin of the Seismological Society of America*, **96**(3), 846-855 (2006)

6. Material and Methods are available as Supplementary Materials on Science Online

7. S. D. Davis, C. Frohlich. Did (or will) fluid injection cause earthquakes?-criteria for a rational assessment. *Seismological Research Letters*, **64**(3-4), 207-224 (1993).

8. C. Frohlich, K. D. Apperson. Earthquake focal mechanisms, moment tensors, and the consistency of seismic activity near plate boundaries. *Tectonics*, **11**, 279–296 (1992).

9. G.P. Hayes, R. W. Briggs, A. Sladen, A., E. J. Fielding, C. Prentice, K. Hudnut, P. Mann, F. W. Taylor, A. J. Crone, R. Gold, T. Ito, M. Simons (2010). Complex rupture during the 12 January 2010 Haiti earthquake. *Nature Geoscience*, **3**(11), 800-805 (2010).

10. D. Massonnet, M. Rossi, C. Carmona, F. Adragna, G. Peltzer, K. Feigl, T. Rabaute. The displacement field of the Landers earthquake mapped by radar interferometry, Nature, **364**(6433), 138–142 (1993).

11. Y. Okada. Surface deformation due to shear and tensile faults in a half-space. *Bulletin of the seismological society of America*, **75**(4), 1135-1154 (1985).

12. D. L. Wells, K. J. Coppersmith. New empirical relationships among magnitude, rupture length, rupture width, rupture area, and surface displacement. *Bulletin of the seismological Society of America*, **84**(4), 974-1002 (1994).

13. W. L. Ellsworth. Injection-induced earthquakes. *Science*, **341**(6142), 1225942 (2013).

14. K. M. Keranen, M. Weingarten, G. A. Abers, B. A. Bekins, S. Ge. Sharp increase in central Oklahoma seismicity since 2008 induced by massive wastewater injection. *Science*, **345**(6195), 448-451 (2014).

15. R. Westaway. Seasonal seismicity of northern California before the great 1906 earthquake. *Pure and Applied Geophysics*, **159**, 7-62 (2002).

16. F. Grigoli, S. Cesca, E. Priolo, A. P. Rinaldi, J. F. Clinton, T. A. Stabile, B. Dost, M. Garcia-Fernandez, S. Wiemer, T. Dahm. (2017). Current challenges in monitoring, discrimination, and management of induced seismicity related to underground industrial activities: A European perspective. *Reviews of Geophysics*, **55**(2), 310-340.

17. A. McGarr. Maximum magnitude earthquakes induced by fluid injection. *Journal of Geophysical Research: Solid Earth*, **119**(2), 1008-1019 (2014).

18. G. M. Atkinson, D. W. Eaton, H. Ghofrani, D. Walker, B. Cheadle, R. Schultz, R. Shcherbakov, K. Tiampo, J. Gu, R. M. Harrington, Y. Liu, M. vam der Baan, H. Kao (2016). Hydraulic fracturing and seismicity in the Western Canada Sedimentary Basin. *Seismological Research Letters*, **87**(3), 631-647.

19. R. Westaway. Induced seismicity. In *Environmental and Health Issues in Unconventional Oil and Gas Development, Elsevier* 175-210 (2016).

20. A. Mignan, M. Broccardo, S. Wiemer, D. Giardini. Induced seismicity closed-form traffic light system for actuarial decision-making during deep fluid injections. *Scientific Reports*, **7**(1), 13607 (2017).

21. F. Grigoli, L. Scarabello, M. Böse, B. Weber, S. Wiemer, S., J. F. Clinton, (2018). Pick-and waveform-based techniques for real-time detection of induced seismicity. *Geophysical Journal International*. doi:10.1093/gji/ggy019, (2018)

22. K. H. Cho, R. B. Herrmann, C. J. Ammon, K. Lee. Imaging the upper crust of the Korean Peninsula by surface-wave tomography. *Bulletin of the seismological Society of America*, **97**(1B), 198-207 (2007).

23. F. Grigoli, S. Cesca, L. Krieger, M. Kriegerowski, S. Gammaldi, J. Horalek, E. Priolo, T. Dahm. (2016). Automated microseismic event location using master-event waveform stacking. *Scientific reports*, **6**, 25744 (2016).

24. X. Chen, N. Nakata, C. Pennington, J. Haffener, J. Chang ,X. He., Z. Zhan, S. Ni, J. Walter (2017). The Pawnee earthquake as a result of the interplay among injection, faults and foreshocks. *Scientific Reports*, **7**(1), 4945.

25. C. Bassin, G. Laske, G. Masters. The current limits of resolution for surfacewave tomography in North America. *Eos. Trans. AGU*, **81**, F897 (2000).

26. R. Wang. A simple orthonormalization method for stable and efficient computation of Green's functions. *Bulletin of the Seismological Society of America*, *89*(3), 733-741 (1999)

27. S. Cesca, S. Heimann, M. Kriegerowski, J. Saul, T. Dahm. Moment Tensor Inversion for Nuclear Explosions: What can we learn from the 6 January and 9 September 2016 Nuclear Tests, North Korea? *Seismological Research Letters*, **88**(2A), 300-310 (2017)

28. G.M. Atkinson, D. M. Boore. Earthquake Ground-Motion Prediction Equations for Eastern North America. *Bulletin of the seismological Society of America, 96*, 2181–2205 (2006).

29. C. Cauzzi, E. Faccioli, M. Vanini, A. Bianchini. Updated predictive equations for broadband (0.01–10 s) horizontal response spectra and peak ground motions, based on a global dataset of digital acceleration records. *Bulletin of Earthquake Engineering, 13*, 1587–1612, (2015).

30. J. Douglas, B. Edwards, V. Convertito, N. Sharma, A. Tramelli, D. Kraaijpoel, B. M. Cabrera, N. Maercklin, C. Troise. Predicting Ground Motion from Induced Earthquakes in Geothermal Areas. *Bulletin of the seismological Society of America, 103*, 1875–1897 (2013).

31. A. Emolo, N. Sharma, G. Festa, A. Zollo, V. Convertito, J. Park, H. Chi, I. Lim, 2015. Ground- Motion Prediction Equations for South Korea Peninsula. *Bulletin of the seismological Society of America, 105*, 2625–2640 (2015).

32. C. B. Worden, M. C. Gerstenberger, D. A. Rhoades, D. J. Wald, 2012. Probabilistic Relationships between Ground- Motion Parameters and Modified Mercalli Intensity in California. *Bulletin of the seismological Society of America ,102*, 204–221 (2012).

33. S. Cesca, S. Heimann, K. Stammler, T. Dahm, 2010. Automated procedure for point and kinematic source inversion at regional distances. *Journal of Geophysical Research, 115*, B06304, (2010).

34. X. He, X., S. Ni, 2018. Resolving Horizontal Rupture Directivity of Moderate Crustal Earthquake in

Sparse Network With Ambient Noise Location, J. Geophys. Res., doi: https://doi.org/10.1002/2017JB014735

35. J. A. Lopez Comino, D. Stich, J. Morales, A M. G. Ferreira. Resolution of rupture directivity in weak events: 1-D versus 2-D source parameterizations for the 2011, Mw 4.6 and 5.2 Lorca earthquakes, Spain. *Journal of Geophysical Research*, *121*(9), 6608-6626 (2016).

36. J. A. Lopez Comino, F. D. L. Mancilla, J. Morales, D. Stich Rupture directivity of the 2011, Mw 5.2 Lorca earthquake (Spain). *Geophysical Research Letters*, *39*(3), L03301, (2012)

37. Uchide, T., and Song, S. G., 2018. Fault rupture model of the 2016 Gyeongju, South Korea, earthquake and its implication for the underground fault system. Geophysical Research Letters, 45, 2257–2264. https://doi.org/10.1002/2017GL076960

38. M. Costantini. A novel phase unwrapping method based on network programming, *IEEE Trans. Geosci. Remote Sens.*, *36*(3), 813–821 (1998).

39. A. Manconi, T. R. Walter, M. Manzo, G. Zeni, P. Tizzani, E. Sansosti, R. Lanari. On the effects of 3-D mechanical heterogeneities at Campi Flegrei caldera, southern Italy, *Journal of Geophysical Research*, *115*(B8), B08405, (2010).

Supplementary Materials:

Supplementary text

Figures S1-S12

Waveform data (local accelerometer)
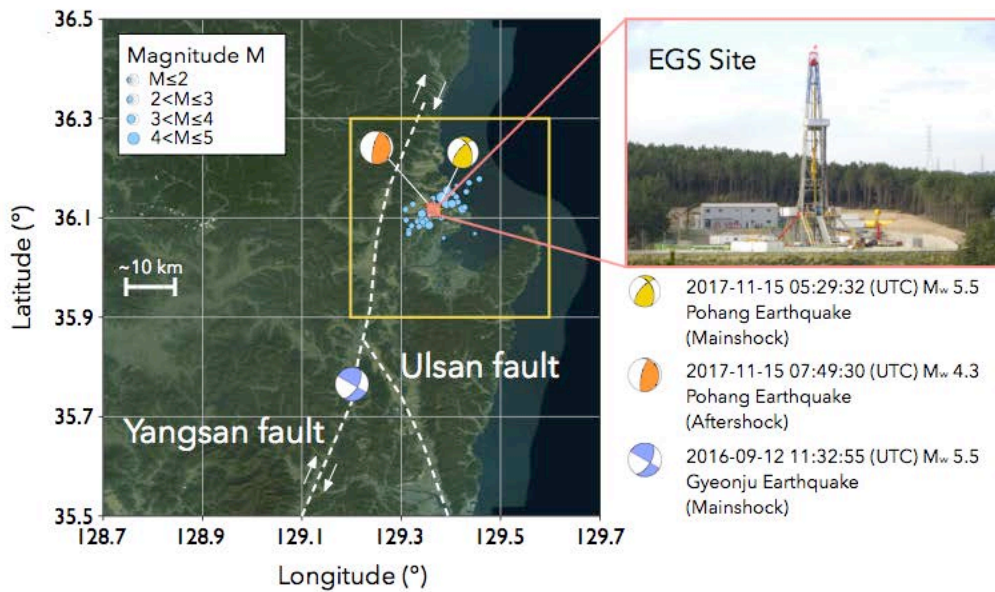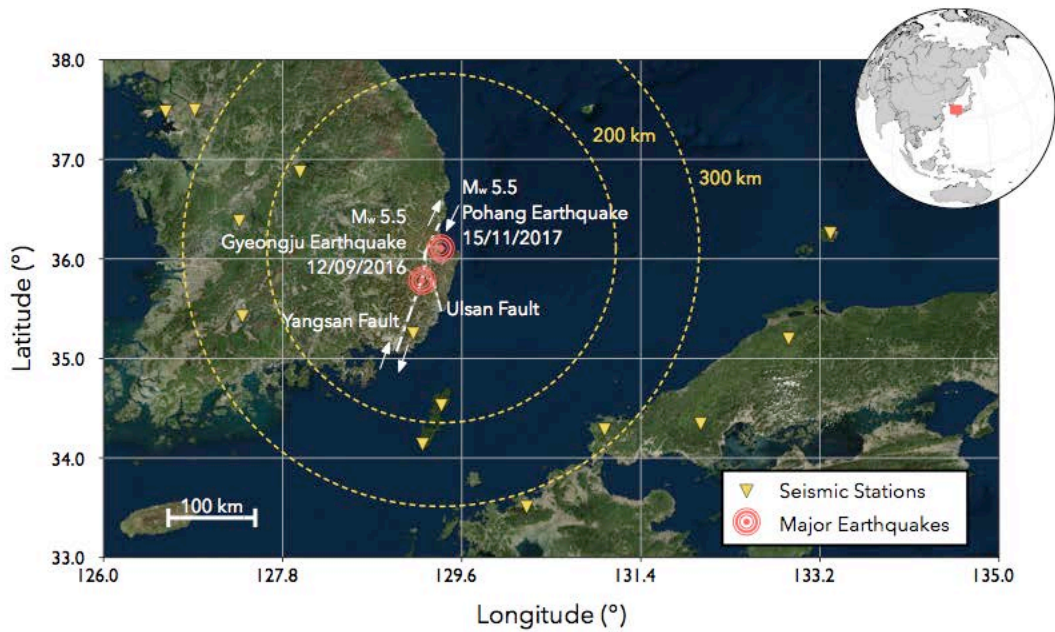
References (*21-39*)

5

10

Fig. 1 The 2016 and 2017 Mw 5.5 South Korea earthquakes. (A) Regional map showing locations of the Gyeongju and Pohang earthquakes, the Yangsan Fault, and the available open seismic stations. (B) Map of the study area showing the main faults of the area, the distribution of seismicity with respect to the EGS site and the mechanisms of the largest events. A more detailed map of the area of study (represented by the yellow square) is shown in Fig. 2A.
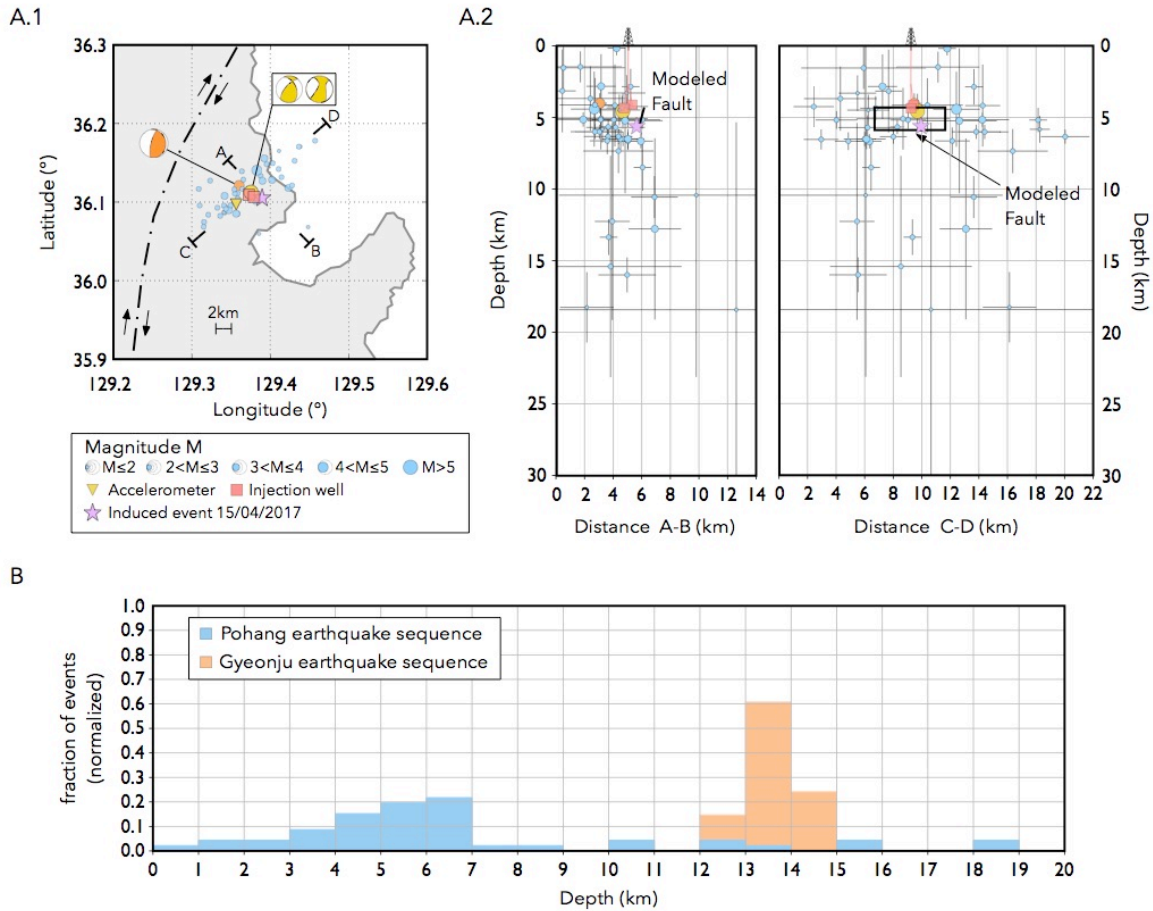
5

Fig. 2 Spatial distribution of the 2017 Pohang seismic sequence. (A.1) Detailed map showing the epicentral distribution of seismicity and (A.2) two cross sections displaying depth distribution of seismicity (including location uncertainties) and the fault as inferred by geodetic analysis. The EGS site is located at 36°06'23.34''N, 129°22'46.08''E and includes the two injection wells that reach depths of 4127 m and 4348 m (3). (B) Focal depth distribution of earthquakes in the study region and comparison with the 2016 Gyeonju seismic sequence. Blue and orange histograms refers to the Pohang and Gyeonju (2) seismic sequences respectively.
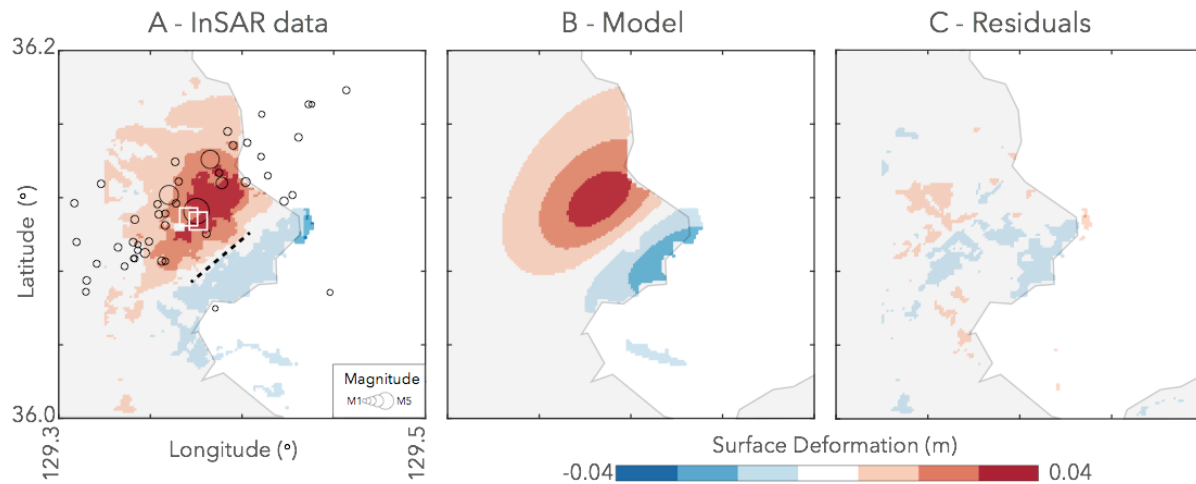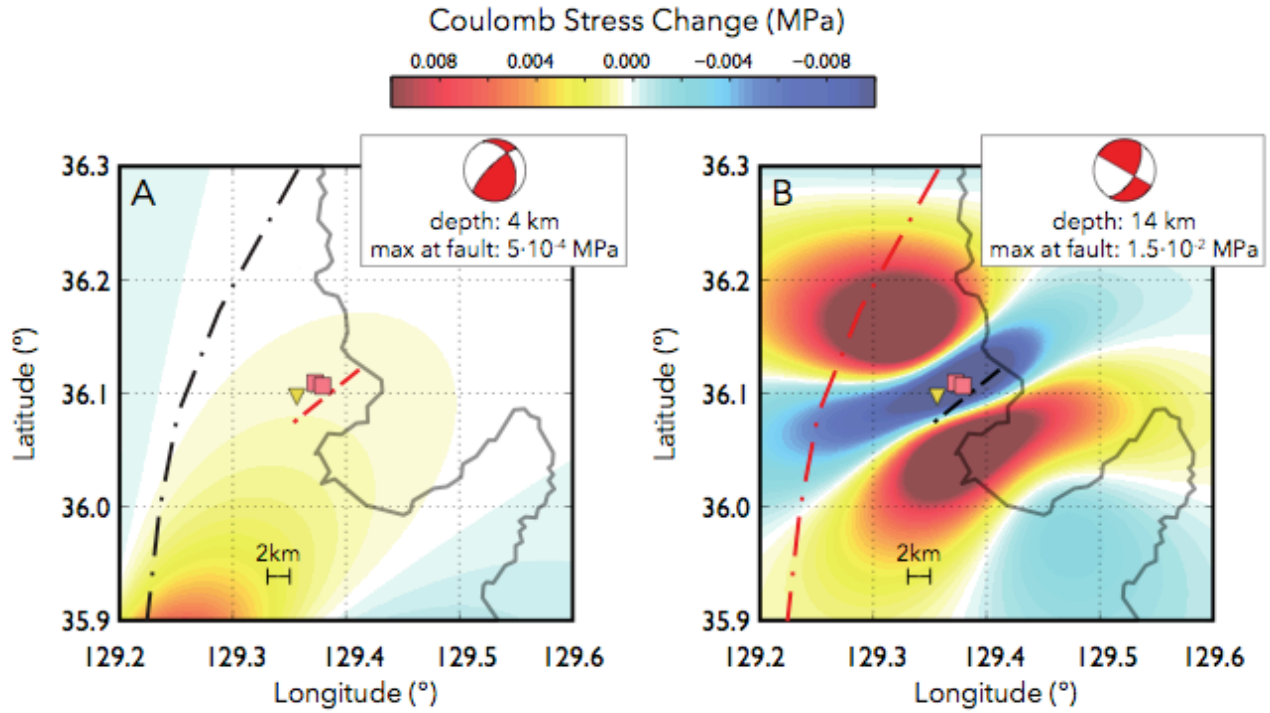
10

Fig. 3. DInsar data and model: (A) Surface deformation (satellite Line-of-Sight displacements) obtained using DInSAR. eismicity and extrapolated fault trace are indicated by black circles and dashed line respectively. (B) Modeled surface deformation using a rectangular fault plane with the following parameters: Lat= 36.100; Lon=129.383 (center of the rectangular fault); Depth=4.3 km (upper edge of the fault) Strike (from North) = 225°; Dip (from horizon) = 75°; Length=~5 km; Width= ~1.6 km; Slip= ~1m; Rake=123°. (C) Difference between DInSAR data and model, i.e. Residuals. Standard deviation <0.5 cm, thus below the accuracy threshold of the measurements.

Fig. 4. Coulomb stress modeling. (A) Static Coulomb Failure Stress showing the effect of the 2016 Gyeonju earthquake at 4 km depth on the fault activated by the 2017 Pohang event and (B) the effect of this latter on the Yangsan fault at 14 km depth.